ELSEVIER

Biochimica et Biophysica Acta 1416 (1999) 176–194

BIOCHIMICA ET BIOPHYSICA ACTA
BBA

Structure, orientation and affinity for interfaces and lipids of ideally amphipathic lytic $L_iK_j(i=2j)$ peptides

Sabine Castano [a], Bernard Desbat [b], Michel Laguerre [a], Jean Dufourcq [a,*]

[a] *Centre de Recherche Paul Pascal, CNRS, Avenue A. Schweitzer, 33600 Pessac, France*
[b] *Laboratoire de Physico-Chimie Moléculaire, Université de Bordeaux I, 33400 Talence, France*

Received 3 June 1998; received in revised form 1 October 1998; accepted 6 November 1998

Abstract

The behavior of lytic ideally amphipathic peptides of generic composition $L_iK_j(i=2j)$ and named LK_n, $n=i+j$, is investigated in situ by the monolayer technique combined with the recently developed polarization modulation IR spectroscopy (PMIRRAS). A change in the secondary structure occurs versus peptide length. Peptides longer than 12 residues fold into α-helices at interfaces as expected from their design, while enough shorter peptides, from 9 down to 5 residues, form intermolecular antiparallel β-sheets. Analysis of experimental and calculated PMIRRAS spectra in the amide I and II regions show that peptides are flat oriented at the interfaces. Structures and orientation are preserved whatever the nature of the interface, air/water or DMPC monolayer, and the lateral pressure. Peptide partition constants, K_{aff}^{Π}, are estimated from isobar surface increases of DMPC monolayers. They strongly increase when Π decreases from 30 mN/m to 8 mN/m and they vary with peptide length with an optimum for 12 residues. This non-monotonous dependence fits with data obtained in bilayers and follows the hemolytic activity of the peptides. Lipid perturbations due to peptide insertion essentially detected on the PO_4^- and CO bands indicate disorder of the lipid head groups. Lysis induced on membranes by such peptides is proposed to first result from their flat asymmetric insertion. © 1999 Elsevier Science B.V. All rights reserved.

Keywords: Cytolytic peptide; FT-IR spectroscopy; Monolayer; Lipid–peptide interaction; Amphipathic peptide; β-Sheet at interface; α-Helix at interface

1. Introduction

Over the past decades, a wide range of cytotoxic peptides have been isolated from the defense systems of various species. Some of them display specific antimicrobial activities like magainins and cecropins, while others kill all types of cells like melittin [1]. It is now well established that these peptides enhance the permeability of biological membranes via direct interaction with the lipid matrix [2–4]. They generally display a positive net charge and a high amphipathic propensity that allow them to adopt amphipathic secondary structures in membrane environment.

Because of this amphiphilic character, numerous natural peptides like melittin [5], δ-hemolysin [6], bombolittin [7] and defensin [8] are surface active and spontaneously form rather stable films at the air/water interface. Monomolecular films formed at the interface of a Langmuir trough provide a unique and convenient model to try to understand at least some steps of the action mechanism of such peptides by studying both pure peptide films at the air/water

* Corresponding author. Fax: +33 5 56 84 56 00; E-mail: dufourcq@crpp.u-bordeaux.fr

0005-2736/99/$ – see front matter © 1999 Elsevier Science B.V. All rights reserved.
PII: S0005-2736(98)00220-X

interface and the peptide insertion into phospholipid monolayers spread at the interface [9]. Though a phospholipid monolayer cannot account for the membrane behavior since it has a different symmetry, this well-oriented planar system is particularly well suited to study the lipid affinity and the structure of peptides.

It has been claimed for a long time that there is no direct relation between surface and biological activities. Synthetic melittin analogues and fragments have proved that hemolytic activity can be totally lost while the peptides are still tensioactive [10]. Similarly an unfolded cardiotoxin without hemolytic activity is more surface active than the native toxin [11]. About the general synergism of such peptides for activation of phospholipase, melittin and sea anemone toxin II have similar surface activities but different abilities to increase PLA_2 activity, while toxins II and III, which have similar hydrophobicities, have different synergistic activities [12]. Melittin and the L_iK_j peptides studied herein have a rather similar synergistic ability to activate bee venom phospholipase A_2 [13]. Then all active peptides have to be tensioactive, but this is not sufficient to give lytic activity.

The secondary structure of such amphipathic molecules strongly modulates their lytic activity. An abundant literature has now established α-helix as a major requirement for cell lysis [14,15]. β-Sheet structures are also often involved but with very different peptides [1,14]. First designed with a minimalist approach, $L_iK_j(i=2j)$ peptides lyse erythrocytes and fold into α-helices [16,17]. Correlation between the helicity on lipid membrane and the hemolytic activity was also established for other types of LK peptides [18]. More recently a short linear β-sheeted L_iK_j peptide has also proved to be hemolytic [19].

Peptides orientation and packing at the interfaces are also determinant factors for the mechanism of action. Several antagonist models called either 'rafts', 'carpets' or 'bundles' [20–22] have been proposed. Peptides can stand with their helix axis (i) either parallel to the interface as for magainin 2 [23,24] or the 22 residue long $L_iK_j(i=2j)$ [17] or (ii) perpendicular to the interface by making bundles thus generating transient channels or holes of variable size [25–27]. Intermediates can be considered by variations of the angle between the molecular axis and the interface [28]. Unfortunately peptide orientation still remains controversial and it can change according to experimental conditions, for instance the sample's hydration degree critically modulates both secondary structure and orientation, as observed for melittin by infrared spectroscopy [25,29]. Therefore in situ and non-invasive characterization at the air/water interface is primordial. But the observation of IR spectra in these conditions is difficult because of the water absorption band. Using D_2O in the subphase, internal reflection absorption (IRRAS) set-ups were successful to obtain proper structures both for lipids and proteins and their reciprocal perturbations [30–32]. Peptides orientation at the interface was documented either by comparing polarized spectra [33] or by direct acquisition of polarization modulated IRRAS (PMIRRAS) spectra [34]. Indeed this technique is powerful to determine peptides conformation and orientation of peptides in situ at the interfaces [17,19,33,35,36] even though secondary structure in lipid monolayers may differ from that in bilayers [37].

In the present paper, correlations between lipid affinity/lytic activity and peptide structure and orientation/lytic activity are studied for a homogeneous series of $L_iK_j(i=2j)$ model peptides with a length of 5–22 residues. With a 2:1 L/K ratio, these peptides are designed to have a single charged K residue per putative α-helical turn to generate ideally amphipathic helices (Fig. 1) [16]. They are strongly lytic towards erythrocytes and liposomes [16,38], and previous PMIRRAS studies showed that the 22 residue long peptide has an α-helical structure [17] while a shorter 9-mer folds into β-sheets [19]. The effects of peptide length on the properties of pure peptide or mixed peptide/DMPC films are systematically inves-

Name	Sequence (1 4 8 11 15 19 22)
$DnsLK_5NH_2$	Dns-K L L L K-CONH2
$DnsLK_8$	Dns-K L L L K L L K
$DnsLK_9NH_2$	Dns-K L L L K L L L K-CONH2
$DnsLK_{12}$	Dns-K L L L K L L L K L L K
$DnsLK_{15}$	Dns-K L L K L L L K L L L K L L K
$DnsLK_{19}$	Dns-K L L L K L L K L L L K L L L K L L K
$DnsLK_{22}$	Dns-K L L K L L L K L L K L L L K L L L K L L K
ia-$LK_{15}W_{14}$	K L L K L L L K L L L K L W K

Fig. 1. Sequence and usual names of the $L_iK_j(i=2j)$ peptide series.

tigated at the air/water interface to quantitatively (i) define the peptide affinity for interfaces, (ii) determine the peptides' structures and orientations and (iii) settle correlations between peptides' physical properties (hydrophobicity, structure, orientation) and lytic activities.

2. Materials and methods

2.1. Materials

Peptides of 5–15 residues were provided by Neosystem (Strasbourg, France), longer ones synthesized by Fournier Pharma (Heidelberg, Germany) [16], all had a purity higher than 97% on HPLC and their masses agreed with the calculated ones. They were stored as dry powders at −20°C and dissolved in MeOH to give stock solutions of about 0.3 mM. The peptide concentrations were estimated from absorbance measurements on a Pye Unicam Philips 8800 spectrophotometer. For dansylated peptides $\varepsilon^{Dns}_{340nm} = 4640\ M^{-1}\ cm^{-1}$, for W containing peptides $\varepsilon^{W}_{280nm} = 5600\ M^{-1}\ cm^{-1}$ [38,39].

Dimyristoylphosphatidylcholine (DMPC) and a fully deuterated analogue (d_{54}-DMPC) from Avanti Polar Lipids (Birmingham, AL) were solubilized in chloroform at about 5 mM.

The organic solvents MeOH and $CHCl_3$, purchased from Prolabo, and Tris from Sigma are the purest available.

2.2. Film formation and surface pressure measurements

The experiments were performed on a computer controlled Langmuir film balance (Nima Technology, Coventry, UK). The rectangular trough (110 cm^3, 145 cm^2) and the barrier are made of teflon. The surface pressure (Π) was measured by the Wilhelmy method using a filter paper plate. Experiments at constant area were carried out on a smaller circular trough (7 cm^3, 28.5 cm^2) to limit the peptide consumption. Troughs were filled with an aqueous buffer (20 mM Tris, 130 mM NaCl, HCl, pH = 7.5) using ultrapure water (Milli-Q, Millipore) and $T = 25 \pm 2$°C.

A few μl of MeOH peptide stock solutions were injected in the subphase to define the total peptide concentration. Compression isotherms and compression/expansion cycles were performed by moving the barrier at 5 cm^2/min.

To obtain mixed peptide/DMPC films, pure DMPC was first spread at the air/water interface from chloroform solutions using a Hamilton microsyringe to reach lateral pressures of 2–3 mN/m. At pressure equilibrium, after ∼15 min, the phospholipid film was compressed (5 cm^2/min) up to the selected pressure, 8 mN/m or 30 mN/m. A few μl of concentrated peptide solutions were then progressively injected into the subphase and the surface increases (ΔS) were registered at each peptide concentration after 30–40 min.

2.3. Estimate of partition coefficients and affinities for interfaces

From the analysis of the $\Pi = f(c)$ curves at the air/water interface, one can extract a partition constant of the peptides between the bulk phase and the interface ($K_p^{A/W}$). Since $\Pi = f(c)$ curves saturate at Π_{max}, C_{lim} is defined as the minimal peptide concentration allowing interface saturation. $K_p^{A/W} = N_p^s / N_p^v$, where the number of peptide molecules at the interface $N_p^s = S_{trough}/S_{mol}$ and the number of peptide molecules in the bulk phase $N_p^v = C_{lim} \times V_{trough} \times N_{av} - N_p^s$ and $N_{Av} = 6.02 \times 10^{23}$.

A partition constant (K_{aff}^{Π}) for the transfer of peptide from the aqueous solution into the lipid monolayer is extracted from the plots $\Delta S/S_0 - f(c)$ for selected lateral pressures (8 mN/m or 30 mN/m). The classical definition for a peptide/bilayer interaction is used [9]:

$$K_{aff}^{\Pi} = \frac{C_b^p}{C_f^p \times C_L^0},\ with\ C_b^p = \frac{\Delta S}{S_{mol} N_{av} V},$$

$$C_L^0 = \frac{S_0}{A_L^{\Pi} N V}\ and\ C_f^p = C_{total}^p - C_b^p$$

C_b^p, the concentration of bound peptide in the total subphase volume (100 ml), is estimated assuming that (i) the total surface results from additivity rules and (ii) the molecular surface of each compound at the interface is constant along the binding process; S_{mol} is the molecular surface of the peptide; N_{Av} = Avogadro number.

C_L^0, the lipid concentration, is calculated as S_0/A_L^Π, the ratio of the initial surface of spread DMPC by the molecular area of DMPC at a defined Π (at 8 mN/m, $A_L^8 = 82.5$ Å^2; at 30 mN/m, $A_L^{30} = 60$ Å^2 [40]).

C_f^p, the concentration of free peptide in the subphase.

The relation between K_{aff}^Π and the P_p^Π slopes of the $\Delta S/S_0 = f(c)$ plots is then defined as follows:

$$K_{aff}^\Pi = P_p^\Pi \times \frac{C_{total}^p \times \frac{A_L^\Pi}{S_{mol}}}{(C_{total}^P - \frac{\Delta S}{S_{mol} N_{Av} V})}$$

2.4. FT-IR spectroscopy measurements

Absorbance spectra of bulk samples of pure peptides were obtained by conventional transmission spectroscopy from a methanolic solution evaporated on a ZnSe window.

At the air/water interface, peptides and mixed peptide/DMPC monolayers were studied in situ by PMIRRAS [34,41]. Spectra were recorded on a Nicolet 740 spectrometer equipped with a HgCdTe detector cooled at 77 K, generally 200 or 300 scans were pooled at resolution of 4 cm^{-1} or 8 cm^{-1} for pure peptide or mixed peptide/DMPC monolayers respectively. Briefly, PMIRRAS combines FT-IR reflection spectroscopy with fast modulation of the incident beam between parallel (p) and perpendicular (s) polarization. The two-channel processing of the detected signal gives the differential reflectivity spectrum $\Delta R/R = (Rp - Rs)/(Rp + Rs)$. To remove the contribution of liquid water absorption, the spectra are divided by those of the subphase. With an incidence angle of 75°C, transition moments in the interface plane give strong and upward oriented bands, while transition moments perpendicular to the interface give weaker and downward oriented bands [34,41].

The decomposition of the amide I and amide II spectral region (1500–1800 cm^{-1}) into individual bands was performed with the Peaksolve software (version 3.0, Galactic) and analyzed as a sum of Gaussian/Lorentzian curves, with consecutive optimization of amplitudes, band positions, half-width and composition of the individual bands.

3. Results

3.1. Peptide monolayers at the air/water interface

3.1.1. Compression isotherms

When a few µl of the peptide stock solutions are injected in the subphase, surface pressure changes indicate peptide surface activity. To reach an initial pressure equilibrium of about $\Pi = 2$–3 mN/m bulk concentrations of 40 ± 5 nM are necessary for the longer peptides ($n \geq 12$) while decreasing the peptide length requires an increase of concentration (Table 1). Then if longer peptides display a comparable surface activity, the latter decreases for peptides shorter than 12 residues. The addition of 130 mM NaCl in the subphase favors the rising of the peptide at the air/water interface by reducing the electrostatic repulsions [34].

The shape of the compression isotherms are quite

Table 1
Characteristic data of pure peptide films and critical pressure ($\Delta\Pi_c$) for peptide insertion into DMPC monolayers and peptide affinity for the air/water interface, $K_p^{A/W}$

Peptide	c (nM)	$\Delta\Pi_S$ (mN/m)	S_Π (cm^2)	$\Delta\Pi_{Coll}$ (mN/m)	$\Delta\Pi_{max}$ (mN/m)	$\Delta\Pi_c$ (mN/m)	$K_p^{A/W}$
$DnsLK_5NH_2$	150	7.5	70	10 ± 2	10 ± 2	< 30	0.6
$DnsLK_8$	60	16.0	95	25 ± 2	25 ± 2	30–35	3.3
$DnsLK_9NH_2$	–	–	–	–	–	–	5.3
$DnsLK_{12}$	41	25.0	108	37 ± 2	32 ± 2	> 35	2.2
$DnsLK_{15}$	35	28.0	108	35 ± 2	32 ± 2	> 35	1.4
$DnsLK_{19}$	45	31.5	110	34 ± 2	32 ± 2	> 35	–
$DnsLK_{22}$	–	–	–	–	–	–	1.3

c = peptide bulk concentration to reach $\Delta\Pi_0 = 2 \pm 2$ mN/m; $\Delta\Pi_S$ measured at $S = 80$ cm^2; S_Π measured at $\Delta\Pi = 10$mN/m; $\Delta\Pi_{Coll}$ = collapse pressure of pure peptide films; $\Delta\Pi_{max}$ = maximal surface activity obtained on $\Pi = f(c)$ curves; –: not determined.

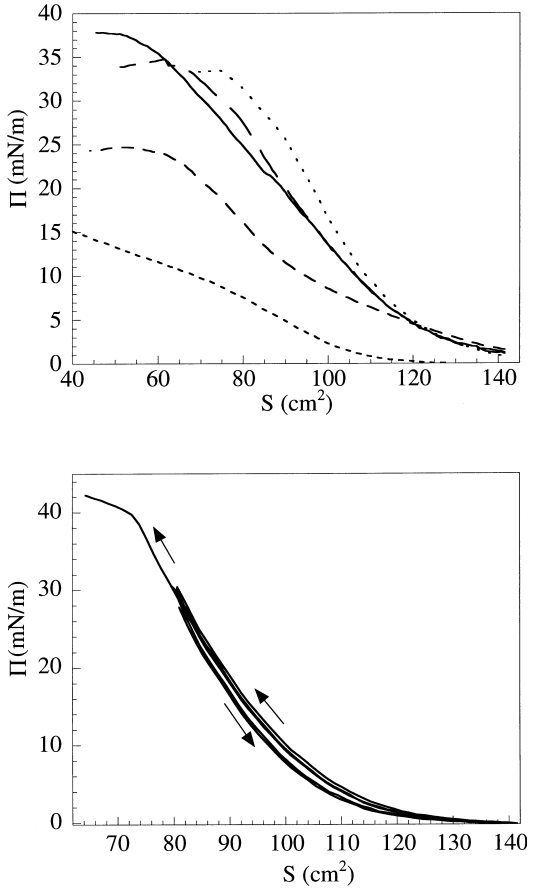

Fig. 2. Peptidic films formed at the air/water interface. (Top) Compression isotherms: short dashes: $DnsLK_5NH_2$ (150 nM); long dashes: $DnsLK_8$ (60 nM); solid line: $DnsLK_{12}$ (41 nM); dot-dashed line: $DnsLK_{15}$ (35 nM); dotted line: $DnsLK_{19}$ (45 nM). (Bottom) Compression/expansion cycles of a $DnsLK_{15}$ film. Peptide concentration: 25 nM. Subphase: 20 mM Tris, 130 mM NaCl, HCl, pH = 7.5, T = 25°C.

similar for the longer peptides ($n \geq 12$) but differ when the length decreases from 12 to 5 residues (Fig. 2). The areas (S_Π), measured at 10 mN/m for the various peptides, increase concurrently with length from 5 to 12 amino acids then reach a plateau for longer peptides (Table 1). Since S_Π is proportional both to the number of peptide molecules at the interface (n) and to the molecular area (S_{mol}) of each peptide, its increase necessarily results from S_{mol} and/or n increase. Similarly at a given area (80 cm^2) Π_S increases concurrently with peptide length from 5 to 12 residues to reach a quasi-plateau for the longer peptides (Table 1).

The collapse pressure (Π_{coll}) of the various peptide films also increases with length from 5 to 12 residues (Fig. 2, Table 1) and reaches a plateau ($\Pi_{coll} = 35 \pm 2$ mN/m) for lengths ≥ 12. As a comparison, the 26 residue long natural melittin gives a lower value, $\Pi_{coll} = 22 \pm 2$ mN/m (data not shown), in agreement with the literature ($\Pi_{coll} = 24.5$ mN/m [42,43]).

Isotherms are reversible in the 0–30 mN/m pressure domain as shown for instance for $DnsLK_{15}$ (Fig. 2, bottom), the film at the interface is in the equilibrium state. But for the 5-mer, at high compressions, a slow quasi-monotonous increase of Π does not make it possible to reach a well defined collapse plateau.

3.1.2. $\Pi = f(c)$ measurements

Performed to investigate the relative affinity of $DnsL_iK_j (i = 2j)$ for the air/water interface, Π versus peptide concentration curves display a common sigmoidal shape (Fig. 3).

The bulk concentrations (c_Π) required to reach 8 mN/m, for instance, decrease by about sevenfold and a further three-fold when peptide length increases from 5 to 8 residues then from 8 to 12 residues (1 μM, 0.15 μM and 0.05 μM respectively). A plateau is reached for $n \geq 12$ ($c_\Pi = 0.05 \pm 0.01$ μM). Then the peptide's ability to cover the air/water interface increases in the order $DnsLK_5NH_2 < DnsLK_8 < DnsLK_{12} \approx DnsLK_{15} \leq DnsLK_{22}$, in agreement with the results from the compression isotherms (Fig. 2, top). $\Delta\Pi_{max}$ values, corresponding to the maximal surface activity of

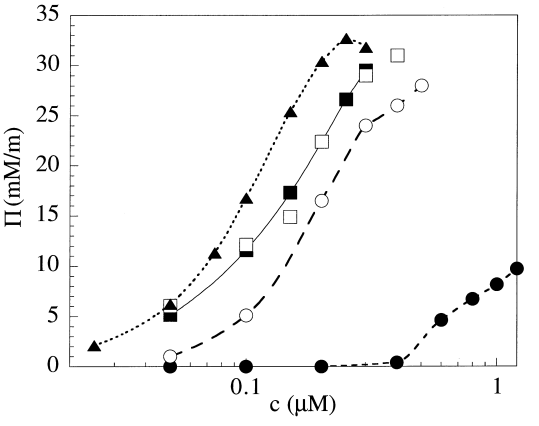

Fig. 3. Surface pressure, Π, changes induced versus bulk peptide concentration: ●: $DnsLK_5NH_2$, ○: $DnsLK_8$, ■: $DnsLK_{12}$, □: $DnsLK_{15}$, ▲: $DnsLK_{22}$. Subphase: 20 mM Tris, 130 mM NaCl, HCl, pH = 7.5, T = 25°C.

each peptide, are quite similar to the Π_{coll} ones (Table 1).

3.1.3. Structure of peptides by PMIRRAS at the air/water interface

PMIRRAS spectra in situ at the interface of pure peptide films of $DnsLK_8$, $DnsLK_{12}$ and $DnsLK_{22}$ clearly show structural changes within the peptide series (Fig. 4, top).

For $DnsLK_8$, a main amide I band is split into a weak band around 1685 cm^{-1} and a sharp and intense one at 1627 ± 2 cm^{-1}, while the amide II mode absorbs at 1540 cm^{-1}. Such frequencies are attributed to antiparallel β-sheet structure [44,45]. $DnsLK_5NH_2$ displays a similar spectrum while for

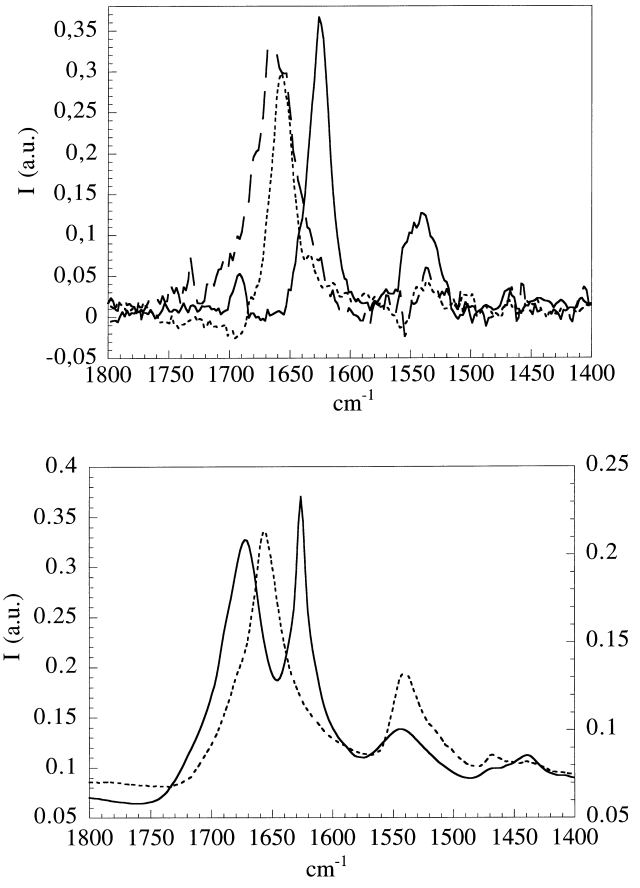

Fig. 4. (Top) PMIRRAS spectra of pure peptide films in situ at the air/water interface: solid line: $DnsLK_8$ 100 nM, Π = 30 mN/m; long dahses: $DnsLK_{12}$ 200 nM, $\Pi = 25$ mN/m; short dashes: $DnsLK_{22}$ 40 nM, $\Pi = 30$ mN/m. Subphase: 20 mM Tris, 130 mM NaCl, HCl, pH = 7.5; $T = 25$°C. (Bottom) IR absorption spectra in bulk state for the amide vibrations domain. Solid line: $DnsLK_8$, dahsed line: $DnsLK_{15}$.

$DnsLK_9NH_2$ the weak contributions around 1673, 1655 and 1645 cm^{-1} (Table 2) are attributed to β-turns, α-helix and random structures respectively [46]. Then short peptides adopt quasi-pure β-sheeted secondary structure at the air/water interface.

The longer peptides ($n \geq 15$) present a strong amide I band at 1657 ± 2 cm^{-1} attributed to α-helix [35,36,46–48] as already found for LK_{22} [17]. For $DnsLK_{12}$, the weak shift to 1661 cm^{-1} of the amide I band and its significant broadening (Fig. 4, top) are due to a more flexible α-helix with looser inter-packing and weaker intramolecular hydrogen bonds [49]. After deconvolution [50–52], the amide I band at 1658 ± 3 cm^{-1} is always well fitted by a dominant contribution of α-helix (Table 2). Though the use of PMIRRAS to a priori quantitatively estimate the relative amounts of structures which can orientate differently is questionable, the relative increase of α-helix content (Table 2) looks significant. Concomitant with length increase from 12 to 22, the amide I band sharpens (Table 2), indicating a stricter helix structuration and a better packing by intermolecular interactions at the interface.

Peptides conformations were also studied by FT-IR absorption spectroscopy in the bulk solid state which is representative of randomly oriented densely packed peptides. For the shorter peptides ($DnsLK_8$ and $DnsLK_9NH_2$), maximum intensities and major components of amide I bands are observed at 1670 cm^{-1} and 1625 cm^{-1} and around 1542 cm^{-1} for the amide II component (Fig. 4, bottom, Table 2). The band around 1670 cm^{-1} is mainly characteristic of β-turns, but can also contain a weak contribution of the TFA counter ions used for the peptide purification [52]. Bands in the 1615–1635 cm^{-1} domain and at 1690 cm^{-1} are typical for β-sheets [44,46,52]. Between 1615 and 1635 cm^{-1}, a convolution of three components at 1635, 1625 and 1615 cm^{-1} likely represents the split amide I vibrational mode of a mixture of parallel (1635 cm^{-1}) and antiparallel β-sheet (1625 and 1615 cm^{-1}) [44,46,52–55]. The weaker component around 1645 cm^{-1} characterizes random structures. For longer peptides ($n \geq 12$), a major amide I component at 1655 ± 3 cm^{-1} can be properly fitted by three individual bands around 1682 ± 2 cm^{-1}, 1655 ± 3 cm^{-1}, 1627 ± 2 cm^{-1} respectively (Fig. 4, bottom, Table 2). The amide II region was decomposed into two modes at 1543 ± 2 cm^{-1} and

Table 2
Positions and assignments of the individual bands resolved in the amide I and amide II domains in FT-IR spectra obtained under various sample conditions for the (Dns)$L_iK_j(i=2j)(NH_2)$ peptide series

Peptide	Sample conditions	Spectral region	cm^{-1}	Relative area (%)[a]	Band width (cm^{-1})[a]	Band assignment
$DnsLK_5NH_2$	air/water interface	amide I	1691-1682	12.0	6.5	β-sheet
	(150 nM $\Pi = 8$ mN/m)		1646	3.0	8.2	random
			1629*-1616	85.2	12.0	β-sheet
	mixed peptide/DMPC	amide I	1690			β-sheet
	film (0.1 μM $\Pi = 30$ mN/m)		1631			β-sheet
		$\nu^{ester}_{(C=O)}$DMPC	1731			
$DnsLK_8$	bulk	amide I	1689	10.0	20.5	β-sheet
			1671*	39.8	25.3	β-turn
			1645	16.9	29.3	random
			1635-1626*-1616	2.5-18.9-11.8	9.8-9.5-17.2	β-sheet
	air/water interface	amide I	1692	5.3	10.2	β-sheet
	(0.1 μM $\Pi = 30$ mN/m)		1626*	94.6	20.9	β-sheet
	mixed peptide/DMPC film	amide I	1691			β-sheet
	(0.1 μM $\Pi = 30$ mN/m)		1624			β-sheet
		$\nu^{ester}_{(C=O)}$DMPC	1735			
$DnsLK_9NH_2$	bulk	amide I	1690	6.4	14.0	β-sheet
			1673*	37.8	30.2	β-turn
			1650	2.5	13.0	random
			1637-1626*-1617	7.6-33.2-12.5	15.2-10.1-17.0	β-sheet
	air/water interface	amide I	1694-1685	19.6	20.0	β-sheet
	(300 nM $\Pi = 21.6$ mN/m)		1667	4.6	13.2	β-turn
			1655	6.0	17.0	α-helix
			1644	9.6	9.8	random
			1628*	60.2	17.4	β-sheet
	mixed peptide/DMPC film	amide I	1690			β-sheet
	(37 nM $\Pi = 30$ mN/m)		1628			β-sheet
		$\nu^{ester}_{(C=O)}$DMPC	1730			
$DnsLK_{12}$	bulk	amide I	1685	18.7	33.4	β-sheet
			1658*	63.7	31.6	α-helix
			1629	17.6	34.3	β-sheet
	air/water interface	amide I	1685	7.9	23.0	β-sheet
	(20 nM $\Pi = 25$ mN/m)		1661*	87.4	36.8	α-helix
			1628	4.8	15.1	β-sheet
	mixed peptide/DMPC film	amide I	1662			α-helix
	(8 nM $\Pi = 30$ mN/m)	$\nu^{ester}_{(C=O)}$DMPC	1735			
$DnsLK_{15}$	bulk	amide I	1684	11.2		β-sheet
			1656*	73.2	28.6	α-helix
			1627	15.1		β-sheet
	air/water interface	amide I	1691	8.2		β-sheet
	(0.2 μM $\Pi = 37$mN/m)		1657*	88.8	29.8	α-helix
			1645	1.8	7.0	random
			1632	1.2		β-sheet
	mixed peptide/DMPC film	amide I	1659			α-helix
	(30 nM $\Pi = 30$ mN/m)	$\nu^{ester}_{(C=O)}$DMPC	1730			
$DnsLK_{22}$	bulk	amide I	1680	10.7		β-sheet
			1655*	81.0	27.3	α-helix
			1625	8.2		β-sheet
	air/water interface	amide I	1680	3.6	11.2	β-sheet
	(40 nM $\Pi = 30$ mN/m)		1656*	72.0	22.4	α-helix
			1632-1615	8.8-15.6	11.0-33.2	β-sheet

(Table continued on next page)

Table 2 (*continued*)

Peptide	Sample conditions	Spectral region	cm^{-1}	Relative area (%)[a]	Band width (cm^{-1})[a]	Band assignment
	mixed peptide/DMPC film	amide I	1659			α-helix
	(8 nM $\Pi = 30$ mN/m)	$\nu^{ester}_{(C=O)}$DMPC	1730			
ia-$LK_{15}W_{14}$	bulk	amide I	1694	10.9	26.6	β-sheet
			1676	13.0	21.0	β-turn
			1657*	52.2	25.3	α-helix
			1632	24.0	30.0	β-sheet
	air/water interface	amide I	1681	4.7	12.0	β-sheet
	(300 nM $\Pi = 21.6$ mN/m)		1659*	75.1	20.8	α-helix
			1632	20.2	32.0	β-sheet
	mixed peptide/DMPC film	amide I	1657			α-helix
	(37 nM $\Pi = 30$ mN/m)	$\nu^{ester}_{(C=O)}$DMPC	1730			

*Major band.
[a]Data from the fits.

1525 ± 2 cm^{-1}. All such features characterize predominant α-helical structures and compare quite well with the literature [36,44,52,54,56]. A comparison of the amide III spectral regions (1350–1200 cm^{-1}) for $DnsLK_{12}$ and $DnsLK_{22}$ (not shown) confirms that $DnsLK_{12}$ is folded into α-helix [57], even if its amide I band is slightly shifted. The two minor bands of the amide I region (with relative area $< 35\%$) are attributable to β-sheet conformations. As observed at the interface, the width of the amide I component at 1655 cm^{-1} decreases while the relative area of the α-helical conformation increases concurrently with peptide length (Table 2).

Then in the bulk state as well as at the air/water interface, the shorter peptides ($n \leq 9$) fold into antiparallel β-sheets while only the longer ones ($n \geq 12$) adopt the expected α-helical structures. For the shorter peptides, the random and β-turn conformations observed in the bulk state are no longer detected at the air/water interface, indicating that the interface induces a more strictly defined structure.

3.1.4. Orientation of peptides by PMIRRAS at the air/water interface

All PMIRRAS spectra of longer peptides ($n \geq 12$) exhibit a strong positive amide I band around 1657 cm^{-1} and a very weak amide II one around 1535 cm^{-1}. The strong AI/AII intensity ratios (≥ 6) are much higher than those observed for the bulk spectra (~ 2.5) indicating an anisotropic peptide orientation at the interface. The amide I band of a pure α-helix can be decomposed into transition moments oriented parallel to the chain axis (A_z) and perpendicular (A_x, A_y). They all absorb around ~ 1655 cm^{-1} but the relative contribution to the intensity of the A_z mode is the strongest [44], then the amide I band of α-helix is mainly due to transition moments oriented parallel to the helix axis. Therefore the tilt angle (θ) of the helix axis compared to the interface normal was estimated from PMIRRAS spectra calculated for different helix orientations [17]. The plot of ratio I_{AI}/I_{AII} versus θ (Fig. 5, top) shows that for $\theta = 90°$ where the main amide I transition moment is in the interface plane, a strong positive amide I band and a weak positive amide II one are expected and correspond to $I_{AI}/I_{AII} \geq 6$. In contrast, an helix perpendicular to the interface ($\theta = 0°$) displays a downward oriented amide I band and a strong positive amide II one which leads to $I_{AI}/I_{AII} < 0$ (Fig. 5, top). Then, $L_iK_j(i = 2j)$ peptides from 12 to 22 residues, with $I_{AI}/I_{AII} \geq 6$, are preferentially oriented with their helix axis parallel to the interface, i.e. with $\theta > 80°$.

Similar analyses were performed for β-sheeted short peptides ($n < 12$) using a general software program [58]. Optical anisotropic index values of the films were generated taking into account the infrared absorptions and dichroism for amide I′ (1685 cm^{-1}), I (1625 cm^{-1}), and II domains measured on spectra of pure β-sheeted peptides. The β-sheet structure can be considered a two-dimensional unit cell with two reference axes corresponding to the average orientations of the amide I′ and amide I transition moments. The amide I′ (1685 cm^{-1}) transition moment is oriented along the peptide chain while

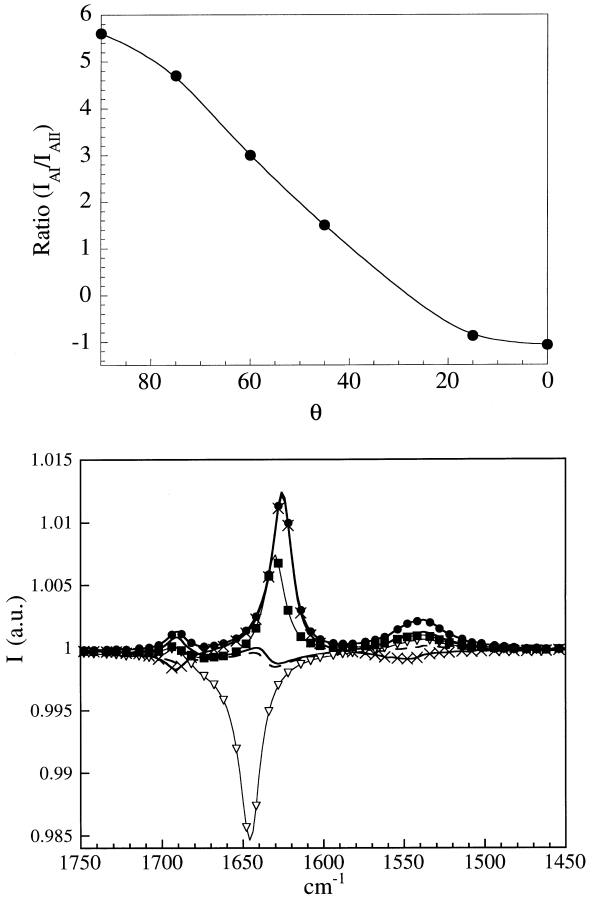

Fig. 5. Calculated PMIRRAS intensities and spectra of amide AI and AII regions according to their orientation compared to the air/water interface plane. (Top) Calculated I_{AI}/I_{AII} ratio for pure α-helices when changing the tilt angle, θ, between the helical axis and the normal to the interface. (Bottom) Set of calculated spectra in amide I and amide II region for pure β-sheets when changing their orientation. θ is the angle between the normal to the interface and the main peptide chain direction, Ψ is the angle between the normal to the interface and the hydrogen bond direction. ●: $\theta=0°$, $\Psi=0°$; solid line: $\theta=45°$, $\Psi=0°$; ▽: $\theta=90°$, $\Psi=0°$; ■: $\theta=45°$, $\Psi=45°$; dotted line: $\theta=90°$, $\Psi=45°$; ×: $\theta=90°$, $\Psi=90°$.

the amide I (1625 cm^{-1}), corresponding to interchain hydrogen bonds, is perpendicular to the former. In the bulk state, the relative intensity ratio $I_{AI(1625cm^{-1})}/I_{AI'(1685cm^{-1})}\sim 10$. Another amide I transition moment (AI″) absorbs around 1670 cm^{-1} and is perpendicular to the β-sheet plane but because of its very weak intensity ($I_{AI(1625cm^{-1})}/I_{AI''(1670cm^{-1})}\gg 20$) [44,59], it was not taken into account. The orientation of a β-sheet initially positioned flat at the interface (amide I′ and amide I transition moments in the plane) is defined by θ representing rotations around the peptide chain axis and ψ traducing rotations around the hydrogen bonds. The calculated spectra for different orientations (Fig. 5, bottom) make it possible to discriminate three extreme orientations of a β-sheet: (i) flat on the interface plane ($\theta=0°$, $\psi=0°$), this gives a weak positive amide I′ (1685 cm^{-1}) band and a strong positive amide I (1625 cm^{-1}) one, resulting in $I_{AI}/I_{AI'}\approx 9$ that is close to what is observed in the bulk state; (ii) perpendicular to the interface with the peptide chains parallel to the interface ($\theta=90°$, $\psi=0°$) that gives a positive amide I′ band and a strong negative amide I one; (iii) perpendicular to the interface with the direction of the interchain hydrogen bonds parallel to the interface plane ($\theta=90°$, $\psi=90°$), this gives a negative amide I′ band and a strong positive amide I one.

The PMIRRAS spectra of the short peptides (Fig. 4, top) display a positive, very sharp and strong band around 1625 cm^{-1} and a positive one around 1685 cm^{-1} indicating transition moments in the interface plane. The ratio values $I_{AI(1625cm^{-1})}/I_{AI'(1685cm^{-1})}>7$ allow us to conclude that the antiparallel β-sheets are roughly flat oriented at the interface.

3.1.5. *Influence of Π on the PMIRRAS spectra at the air/water interface*

Lateral pressure changes may modify the structure, the orientation and the number of molecules of the peptides at the interface, therefore PMIRRAS spectra of DnsLK$_8$, ia-LK$_{15}$W$_{14}$ and DnsLK$_{22}$ were registered at various steps of the pure peptide film compression.

For DnsLK$_8$, whatever the compression state, the two amide I and I′ bands characteristic of a β-sheet are at the same position with the same relative amplitude (Table 3). Similarly for ia-LK$_{15}$W$_{14}$ and DnsLK$_{22}$, the amide I mode at 1659 ± 1 cm^{-1} does not depend on Π. Then, the peptide secondary structures at the interface are pressure independent from 10 mN/m up to collapse. At lower pressure the IR spectrum of Dns LK$_8$ shows deformation in the amide I band.

The I_{AI}/I_{AII} and $I_{AI}/I_{AI'}$ ratios are strongly sensitive to the orientation at the interface. $I_{AI}/I_{AII}=6.8\pm1$ for ia-LK$_{15}$W$_{14}$ and DnsLK$_{22}$ remain rather constant and high in the whole pressure domain, similarly $I_{AI}/I_{AI'}=9\pm2$ for DnsLK$_8$ despite

Table 3
Evolution of frequencies and intensities in the amide region of PMIRRAS spectra versus lateral pressure Π

Π (mN/m)	DnsLK$_8$					ia-LK$_{15}$W$_{14}$				DnsLK$_{22}$			
	$\nu_{(AI')}$ (cm^{-1})	$\nu_{(AI)}$ (cm^{-1})	$\nu_{(AII)}$ (cm^{-1})	I_{AI} [a] (a.u.)	$I_{AI}/I_{AI'}$	$\nu_{(AI)}$ (cm^{-1})	$\nu_{(AII)}$ (cm^{-1})	I_{AI} [a] (a.u.)	I_{AI}/I_{AII} [a]	$\nu_{(AI)}$ (cm^{-1})	$\nu_{(AII)}$ (cm^{-1})	I_{AI} [a] (a.u.)	I_{AI}/I_{AII} [a]
6.8	–	–	–	–	–	–	–	–	–	1656	1535	6.940	6.8
10	1689	1625	1540	6.481	7.3	1660	1533	4.820	7.2	–	–	–	–
15	1691	1625	1539	7.063	11.4	1659	1534	4.939	6.7	1656	1535	7.952	7.9
20	1689	1625	1538	6.885	7.5	–	–	–	–	–	–	–	–
25	1692	1625	1540	7.988	11.2	1659	1542	6.369	6.1	1657	1538	8.291	6.9
30	1693	1625	1542	9.375	7.4	1659	1535	6.822	5.8	1657	1537	8.277	7.5
35	–	–	–	–	–	1659	1535	6.926	6.3	1657	1535	8.294	5.1
40	–	–	–	–	–	1658	1536	7.851	5.4	–	–	–	–

DnsLK$_8$ 100 nM; ia-LK$_{15}$W$_{14}$ 65 nM; DnsLK$_{22}$ 40 nM; 20 mM Tris, 130 mM NaCl, HCl, pH = 7.5 buffer.
[a]Integrated area under the main amide I band at ν_{AI} or integrated area under the main amide II band at ν_{AII}.

larger fluctuations (Fig. 6, top). Then peptide orientation at the interface is essentially pressure independent.

Finally, since the peptide structures are constant, the number of molecules present in the film on compression can be monitored through intensity changes. The intensity of amide I band, I_{AI}, is sensitive both to the surface concentration (n/S), where S is the film surface during the compression and n the number of molecules in the film, and to their orientation ($f(\theta)$). Then $I_{AI} \times S$ is proportional to $n \times f(\theta)$. Neither the structure nor the orientation is modified by compression, then $I_{AI} \times S$ will vary directly as n. The $I_{AI} \times S = f(S)$ variations for ia-LK$_{15}$W$_{14}$ and DnsLK$_{22}$ (Fig. 6, bottom) show a quasi-plateau then the peptide film composition is constant in the 10–30 mN/m domain. A decrease for $\Pi > 30$ mN/m parallels the collapse of the film and probably reflects a decrease in the number of molecules in the film. For DnsLK$_8$, the $I_{AI} \times S$ plateau in the 15–30 mN/m pressure domain also shows a constant number of molecules in the film. The increase observed at high surfaces, i.e. $\Pi < 10$ mN/m, may be not significant because of weaker peptide structuration and/or presence of other structures.

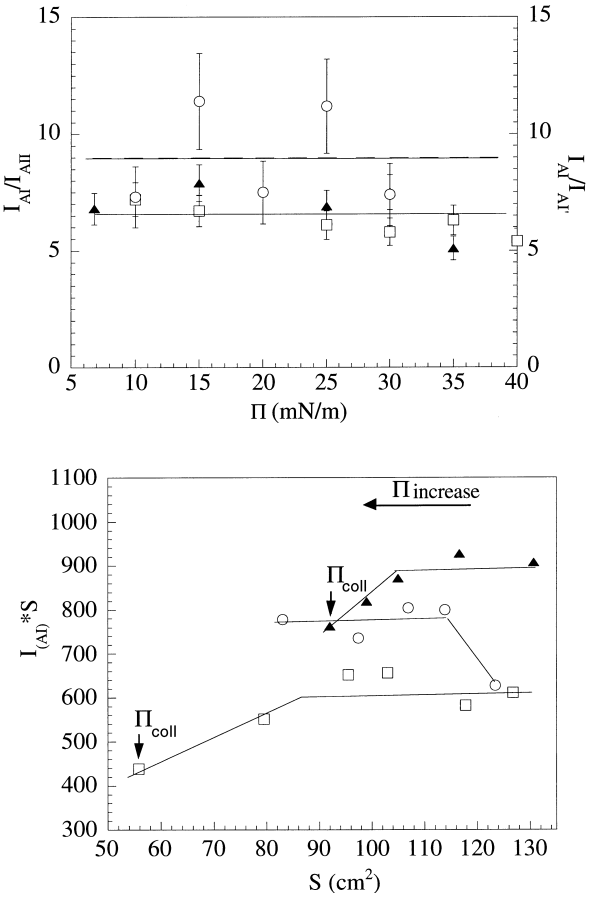

Fig. 6. Changes in the IR vibration band intensities upon film compression. (Top) Plot of intensity ratios I_{AI}/I_{AII} and $I_{AI}/I_{AI'}$ versus lateral pressure, Π. (Bottom) $I_{(AI)} \times S = f(S)$ variations calculated from the PMIRRAS spectra and film surface of pure peptide films during compression (Π_c = collapse pressure). ○: DnsLK$_8$ (100 nM), □: ia-LK$_{15}$W$_{14}$ (65 nM), ▲: DnsLK$_{22}$ (40 nM). Subphase: 20 mM Tris, 130 mM NaCl, HCl, pH = 7.5, T = 25°C.

3.2. Mixed peptide/DMPC films at the air/water interface

3.2.1. Isotherm and isobar insertion of peptides

The lipid affinity of the L$_i$K$_j$($i = 2j$) can be directly monitored through the area increase of a preformed lipid monolayer at constant surface pressure [9]. A

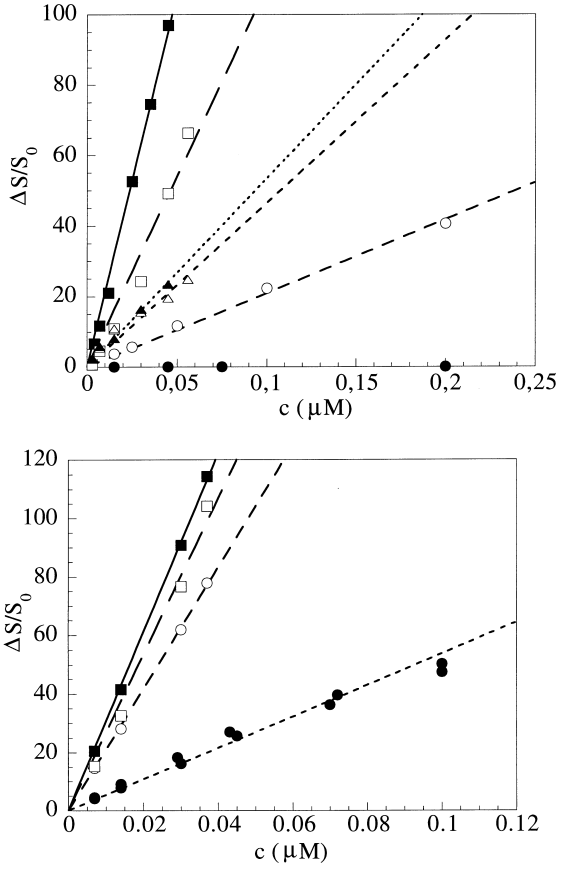

Fig. 7. Relative surface increase on insertion at constant pressure into preformed DMPC monolayers of the $L_iK_j(i=2j)$ peptides on increasing their bulk concentration in the subphase: (top) at $\Pi = 30$ mN/m, (bottom) at $\Pi = 8$ mN/m. ●: $DnsLK_5NH_2$, ○: $DnsLK_8$, ■: $DnsLK_{12}$, □: $DnsLK_{15}$, △: $DnsLK_{19}$, ▲: $DnsLK_{22}$. Subphase: 20 mM Tris, 130 mM NaCl, HCl, pH = 7.5, $T = 25$°C.

DMPC monolayer was first compressed up to $\Pi =$ 30 mN/m, a lateral pressure mimicking lipid bilayers or biological membranes [60,61]. After peptide injection into the subphase, the surface increases were monitored when a constant area was reached at $t \approx 15$ min. The changes of the relative area of the mixed peptide-lipid films ($\Delta S/S_0$) versus total peptide concentration (c) (Fig. 7, top) show that, in the concentration range of 10^{-8}–10^{-6} M, all the peptides out of the shorter 5-mer increase the surface, then they insert into the DMPC monolayer. The experimental data are well fitted by linear plots, the slopes, P_p^{30}, are then proportional to the number of peptide molecules incorporated in the film, i.e. related to their partition coefficient (K_{aff}^{30}) between the DMPC monolayer and the aqueous phase (Table 4). For $DnsLK_5NH_2$, $P_p^{30} = 0$ shows the peptide is unable to insert into the densely packed monolayer up to the maximal concentration assayed. When length increases from 8 to 12 residues, P_p^{30} increases by a factor of 10. P_p^{30} reaches the maximum value for the 12 residue long peptide then it decreases significantly when length increases from 12 to 22 residues (Table 4). Then the peptide's ability to insert into the lipid monolayer compressed at $\Pi = 30$ mN/m does not follow a monotonous evolution versus peptide length.

Insertion at lower pressure, 8 mN/m, shows that $\Delta S/S_0 = f(c)$ plots (Fig. 7, bottom) are again properly fitted by straight lines with quite large slope values, P_p^8, and whatever the peptide $P_p^8 \gg P_p^{30}$ (Table 4). Then, $DnsLK_5NH_2$ inserts efficiently into the loosely packed DMPC monolayer. When the peptide length increases, P_p^8 evolves as already observed at 30 mN/m and the shorter the peptides, the stronger the sensitivity of P_p^{Π} to the initial pressure of DMPC monolayer (Table 4).

3.2.2. PMIRRAS of mixed peptide/DMPC films

First the characteristic absorption bands of DMPC are observed on all the PMIRRAS spectra (Fig. 7, Table 2): $\nu_{C=O}^{ester}$ around 1730 cm^{-1}, δ_{CH2} around 1470 cm^{-1} and $\nu_{P=O}^{antisym}$ around 1255 cm^{-1}. The bands are more intense and better defined at 30 mN/m compared to 8 mN/m because of the better organization of molecules at interface. The peptide insertion into the monolayer always induces a de-

Table 4
Slopes, P_p^{Π}, of the surface increase of the monolayer versus peptide concentration in the subphase, $\Delta S/S_0 = f(c)$, measured for a DMPC monolayer at different lateral pressures, and peptide molecular area, S_{mol}, from geometrical approximations and the PMIRRAS structure and orientation

Peptide	P_p^{30} (μM^{-1})[a]	P_p^8 (μM^{-1})[b]	S_{mol} (Å^2)
$DnsLK_5NH_2$	0	520 ± 20	160
$DnsLK_8$	209 ± 5	2081 ± 20	210
$DnsLK_9NH_2$	1000 ± 10	n.d.	222
$DnsLK_{12}$	2117 ± 42	3055 ± 25	300
$DnsLK_{15}$	1225 ± 30	2670 ± 100	350
$DnsLK_{19}$	464 ± 30	n.d.	422
$DnsLK_{22}$	534 ± 30	n.d.	480

n.d. = not determined.
[a] $\Pi = 30$ mN/m.
[b] $\Pi = 8$ mN/m.

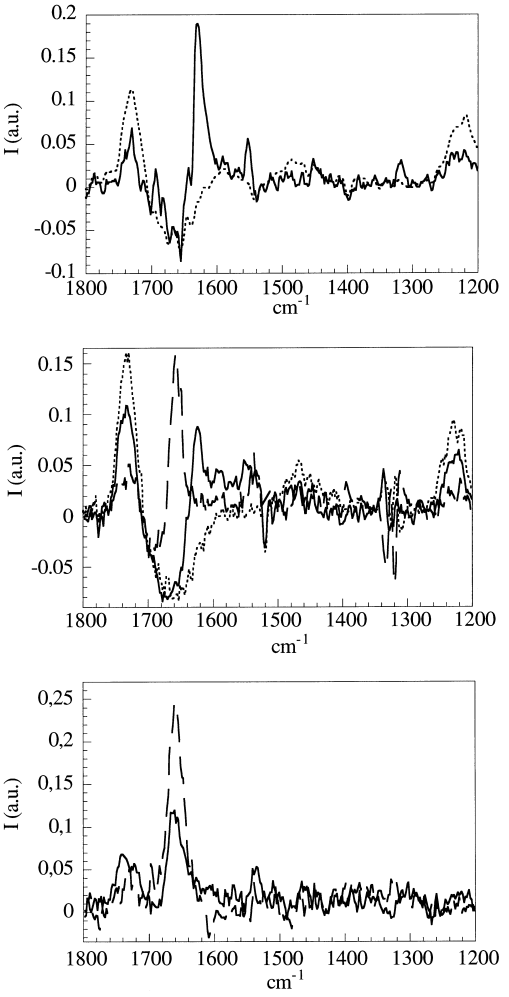

Fig. 8. In situ PMIRRAS spectra of L_iK_j($i=2j$) peptides inserted into a DMPC monolayer. (Top) Dotted line: pure DMPC ($\Pi=8$ mN/m), solid line: mixed $DnsLK_5NH_2$ (100 nM)/DMPC ($\Pi=8$ mN/m). (Center) Dotted line: pure DmPC ($\Pi=30$ mN/m), solid line: mixed $DnsLK_8$ (100 nM)/DMPC ($\Pi=30$ mN/m), dashed line: mixed $DnsLK_{22}$ (8 nM)/DMPC ($\Pi=30$ mN/m). (Bottom) Solid line: mixed $DnsLK_{12}$ (8 nM)/DMPC ($\Pi=30$ mN/m), dashed line: mixed $DnsLK_{15}$ (30 nM)/DMPC ($\Pi=30$ mN/m). Subphase: 20 mM Tris, 130 mM NaCl, HCl, pH = 7.5, $T=25$°C.

crease in the intensities of the characteristic $\nu^{ester}_{C=O}$ and $\nu^{antisym}_{P=O}$ bands.

Since peptides significantly contribute to the film surface, their in situ secondary structure when inserted into the DMPC monolayers can be defined. These spectra are rather similar to those of pure peptide films. For the short $DnsLK_5NH_2$ and $DnsLK_8$ (Fig. 8, top and middle, Table 2), the amide I mode is again split into a weak positive band (AI′) at $\sim$1690 cm^{-1} and a sharp positive and intense one at 1627 ± 4 cm^{-1} (AI) characteristic of antiparallel β-sheets. The value $I_{AI}/I_{AI'}>7$ leads to the conclusion of a flat orientation of the peptides at the interface. For the longer peptides ($n\geq12$, Fig. 8, bottom, Table 2), the amide I absorption around 1660 ± 2 cm^{-1} characterizes an α-helix structure. The weak amide II mode around 1535 ± 5 cm^{-1} in the case of $DnsLK_{12}$ and $DnsLK_{22}$ and its lack for $DnsLK_{15}$ again prove a flat orientation at the interface.

3.2.3. Insertion and PMIRRAS of peptides in deuterated DMPC monolayer

Experiments were performed using d_{54}-DMPC to more carefully investigate the lipid chain behavior during peptide insertion since CD_2 stretching vibrations of fatty acid chains are sensitive to chain order [62]. They are detected at $\nu^{as}_{CD2}\approx2195$ cm^{-1} and $\nu^{s}_{CD2}\approx2095$ cm^{-1} on the PMIRRAS spectra of pure lipid films. At 30 mN/m, $DnsLK_9NH_2$ and $DnsLK_{15}$ insert into the d_{54}-DMPC monolayer very similarly compared to DMPC monolayer ($P^{30}_p=850\pm50$ μM^{-1} and $P^{30}_p=1300\pm100$ μM^{-1} for $DnsLK_9NH_2$ and $DnsLK_{15}$ respectively) and their secondary structures and orientations are those observed in DMPC films (spectra not shown).

No significant wavelength shift is observed for the characteristic d_{54}-DMPC vibration bands but the intensities of all bands decrease because of peptide insertion (Table 5). Whatever the band considered, $-\Delta I/I_0\leq\Delta S/S_0$ means that surface dilution of the lipids is not sufficient to account for the $\Delta I/I_0$ variations, then mixed peptide/d_{54}-DMPC films are probably heterogeneous, with large domains at the interface and/or change in lipid orientation. For $DnsLK_{15}$, $\Delta I/I_0$ is comparable whatever the DMPC band then all DMPC groups are similarly affected by the peptide insertion. Furthermore, at the lower peptide content in the films, the intensity decreases are comparable to surface dilution (Table 5). Then $DnsLK_{15}$ insertion does not induce more isotropic orientation of specific DMPC groups, the DMPC molecules remain well organized in the film. Conversely, for the $DnsLK_9NH_2$, especially at high peptide concentration, $\Delta I/I_0$ significantly varies according to the band considered. Indeed, $\Delta I/I_0$ for $\nu^{ester}_{C=O}$, ν^{as}_{CD2} and ν^{s}_{CD2} are quite comparable (Table 5), while $\Delta I/I_0$ for $\nu^{as}_{PO_4^-}$ is much stronger, meaning that the

Table 5
Changes induced by $DnsLK_9NH_2$ and $DnsLK_{15}$ insertion into a deuterated DMPC monolayer

Peptide	c (nM)	$\Delta S/S_0$ (%)	$-\Delta I/I_0$ (%)			
			$\nu_{C=O}^{ester}$	$\nu_{PO_4^-}$	$\nu_{CD_2}^{as}$	$\nu_{CD_2}^{s}$
$DnsLK_9NH_2$	55	43.9	31.4	46.6	39.5	41.5
	70	58.5	14.6	29.7	14.5	14.0
$DnsLK_{15}$	30	43.0	40.4	40.8	40.3	46.8
	45	68.8	44.0	44.0	40.3	39.2

Film surface changes ($\Delta S/S_0$) and PMIRRAS intensity variations ($-\Delta I/I_0$) of the main DMPC bands were determined for various peptide bulk concentrations.

$DnsLK_9NH_2$ insertion causes a more isotropic orientation of the DMPC head groups without deeper perturbation.

4. Discussion

4.1. Surface activity of the peptides

All the $DnsL_iK_j(i=2j)$ peptides form stable and dense films at the air/water interface, significantly reducing the surface tension of water. The surface activity increases concurrently with length up to 12 residues then reaches a plateau for the longer peptides folded into α-helices at the interface. In the literature, only few L_iK_i peptides have already been studied [63]. Seven residue long Fmoc-LKKLLKL peptide films collapse at 3 mN/m, which is significantly weaker than what is obtained here for the $DnsL_iK_j(i=2j)$ 5- or 8-mer. However, the surface activity of long $DnsL_iK_j(i=2j)$ peptides ($n>12$) is rather similar to that observed for an α-helical 14 residue long $(LKKLLKL)_2$ peptide with a 1:1 L:K ratio [63]. Then the surface activity of such structured peptides depends neither on the length nor on the apolar to polar ratio.

The strong surface activity of the $DnsL_iK_j(i=2j)$ peptides allows their insertion into preformed DMPC monolayers at the air/water interface. The comparison of the slopes P_p^{Π} (Table 4) at 8 and 30 mN/m (Fig. 7) shows the same non-monotonous evolution versus peptide length as observed for tensioactivity. Furthermore, the insertion ability of peptide always decreases when the initial pressure increases (Table 4). An extrapolated critical pressure (Π_c) beyond which there is no more peptide penetration into DMPC monolayer leads to $\Pi_c < 30$ mN/m for $DnsLK_5NH_2$, $\Pi_c \approx 30/35$ mN/m for the 8-mer, and $\Pi_c > 35$ mN/m for the longer 12- and 15-mers (Table 2). For melittin and δ-toxin, $\Pi_c \approx 38$ mN/m with saturated lecithin monolayer [11,64] while for defensin, $\Pi_c \approx 32$ mN/m [8]. Then even the shorter peptides of the $DnsL_iK_j(i=2j)$ series penetrate condensed phospholipid monolayers and the longer ones ($n \geq 12$) behave towards zwitterionic lipids quite similarly to the most active natural cytotoxins. Furthermore, whatever the peptide, $\Pi_{coll} \ll \Pi_c$ illustrates that peptides display a higher affinity for the lipid interface than for free air/water one. Then an optimal lateral pressure of the DMPC film for peptide insertion must exist.

4.2. Peptide structure in situ at the interfaces

PMIRRAS makes it possible to obtain in situ secondary structure and orientation of $DnsL_iK_j(i=2j)$ pure peptide and mixed peptide/DMPC films at the air/water interface, then peptides fold differently according to their length whatever the lateral pressure.

Long peptides (≥12 residues) fold into α-helices at interfaces, in agreement with previous findings of a critical length of about 12 residues for α-helix stability in buffer solution [65]. In contrast, shorter peptides, which are unfolded in solution [66], fold into antiparallel intermolecular β-sheets though the 3.6 periodicity of K in their sequence is adequate for a helical structure but because they are too short to stabilize intramolecular hydrogen bonds. This differs from the studies of (LK) peptides with a ratio L/K = 1 where the periodicity in the sequence imposes the folding into α-helix or β-sheet respectively [63]. Our conclusion agrees better with data in low dielectric solvents where the minimal chain lengths

for α-helix and β-sheet formation are settled at 13 and 4 respectively for amino acid homopolymers [67]. For alternated $(SL)_n$ or $(SVKV)_n$ peptides, the critical length for the formation of β-structures is about 8 residues [68,69].

If β-sheets of the 7 residues long $(LK)_3L$ peptide [63] are ideally amphipathic with all the positive charges segregated on one side of the structure, in $DnsLK_5NH_2$ and $DnsLK_9NH_2$, apolar residues are present on both faces. Then the hydrophobic moments of the β-structure [70], μ_H^β, are weaker than those of ideal $(LK)_n$ β-sheets, but remain considerably higher than those calculated for α-helices (2.73 versus 2.41 for the 5-mer and 4.36 versus 3.44 for the 9-mer respectively). For $DnsLK_8$, the non-ideal secondary amphiphilic feature is well depicted by the low value $\mu_H^\beta \approx 1.63$. Then, for short $DnsL_iK_j (i=2j)$ peptides (<10 residues) surface activity and secondary structure are exclusively controlled by peptide length; contrary to what was previously mentioned in the literature [63,69], neither the hydrophobic periodicity in the amino acid sequence nor the intrinsic ability to form β-structures at the air/water interface are determinant for the formation of stable β-sheets. Furthermore the presence of α-helices is not an essential criterion for the surface activity of proteins [71].

4.3. Peptide orientation in situ at the interfaces

PMIRRAS spectra of the peptides both at the air/water interface and inserted into a DMPC monolayer allowed us to conclude to a flat orientation whatever the lateral pressure, the length and the secondary structure of the peptides.

Nevertheless, β-sheets of short 8- and 9-mers are ~ 30 Å long in the direction of the peptide chain, which would be sufficient to span a bilayer. But the unfavorable hydrophilic/hydrophobic interactions in the bilayer core would be difficult to compensate even by self-association. Therefore the interfacial flat orientation for the β-sheets, confirmed by MD calculations (data not shown), is the most favorable to optimize these interactions.

The longer peptides (≥15 residues) in α-helices are long enough to be transmembranous and then the monolayer model, which reproduces neither the thickness nor the curvature of the bilayer, would not be adequate. But again both PMIRRAS data and MD calculations (data not shown) for a LK_{15} lead to conclude to an α-helix axis parallel to the interface whatever the conditions, as already observed on LK_{22} [17] and in agreement with solid state NMR on oriented bilayers using ^{15}N labelled LK peptides with a 1/1 L/K ratio [72].

Peptide molecular surfaces at the interface, S_{mol}, can be approximated: an antiparallel β-sheet parallel to the interface plane occupies a surface of $n \times 3.4$ Å $\times 4.7$ Å $= 16 \times n$ Å^2, whereas a similarly oriented α-helix occupies $n \times 1.5$ Å $\times 12$ Å $= 18 \times n$ Å^2, where n is the number of residues [73–76], a surface of 80 Å^2 was added to account for the Dns group (Table 4).

4.4. Lipid perturbations and physical state of the films

From ΔS measurements and S_{mol} estimated here above, the lipid to peptide ratio in the films at the interface (R_s) is estimated making the assumptions that molecular areas are simply additive and the lipid and peptide molecular areas are not significantly changed by the presence of the other partner within mixed films. $R_s = N_{pept}/N_{lipid}$, where N_{pept} = number of peptide molecules at the interface $= \Delta S/S_{mol}$ and N_{lipid} = number of DMPC molecules at the interface $= S_0/A_L^\Pi$, S_0 = initial surface of spread DMPC; A_L^Π = molecular area of DMPC at a defined Π (at 30 mN/m, $A_L^{30} = 60$ Å^2 [40]). Then $R_s = 19$, 36, 84 and 120 for the 8-, 12-, 15-, and 22-mer respectively for the PMIRRAS spectra obtained with d_{54}-DMPC (Fig. 8). The intensity decrease of $\nu_{C=O}^{ester}$ (around 1730 cm^{-1}) and $\nu_{P=O}^{antisym}$ (around 1255 cm^{-1}) is correlated neither to the $\Delta S/S_0$ interface increase nor to the R_s ratio variations. For the short peptides (8, 12 residues), whose films are rich in peptide compared to the longer ones (15, 22 residues), greater perturbations of the characteristic phospholipid bands could be expected, but the reverse is observed. Two complementary hypotheses can then be formulated. First, peptide interaction with and insertion into the DMPC monolayer introduce some disorder at the phospholipid interface. Then C=O and P=O vibration moments can adopt a more isotropic orientation that differs according to the peptide structure and R_s. This will lead to a decrease of the band intensity since PMIRRAS is mainly sensitive to anisotropic

orientation. However, even in the case of a total isotropic orientation, the intensity will at worst be divided by two while, for $DnsLK_{15}$ and $DnsLK_{22}$, the bands almost vanish. Second, the formation of inhomogeneous mixed films with a partial segregation into peptide-rich domains and lipid ones could explain the rather arbitrary variations of the characteristic phospholipid bands. Experiments performed on deuterated DMPC monolayer accredit the probably existence of large domains in the case of β-sheeted and α-helical peptides. Furthermore, when the compression cycles of the mixed films are completed (from 30 down to 20 then to 30 mN/m), some phospholipid characteristic bands reappear. This can result from a homogenization of the films (results not shown).

Insertion into d_{54}-DMPC monolayers and MD calculations (data not shown) show that the perturbations on the lipids are different according to the peptide secondary structures. β-Sheeted peptides do not penetrate deeply into the monolayer, inducing a more isotropic orientation only of the PO_4^- lipid groups. Conversely, the longer α-helical peptides strongly perturb the C=O ester group but without severe disorder of the lipid chains. All happens as if the peptides push some lipid molecules, probably leading to weak changes in the molecular area per lipid in the presence of peptides in the films.

4.5. Peptide affinities for the interfaces

The partition constants, $K_p^{A/W}$, of the peptides between the bulk phase and the air/water interface follow an unexpected behavior in the $DnsL_iK_j(i=2j)$ series (Fig. 9): $K_p^{A/W}$ increases with length up to a maximum for the 9-mer then it slightly decreases to reach a plateau value for $L>15$. This biphasic evolution, different from the expected monotonous increase of the affinity versus peptide length, can be explained both by the self-association process that occurs when length increases [15,38] and by the changes in the secondary structure and then the location of the peptides at the interface documented herein. For shorter peptides ($L\leq 12$), which are mainly monomers in the bulk phase [38], the affinity increases with peptide hydrophobicity. Longer peptides ($L\geq 15$) oligomerize in the subphase [38], then the self-association equilibrium competes with the

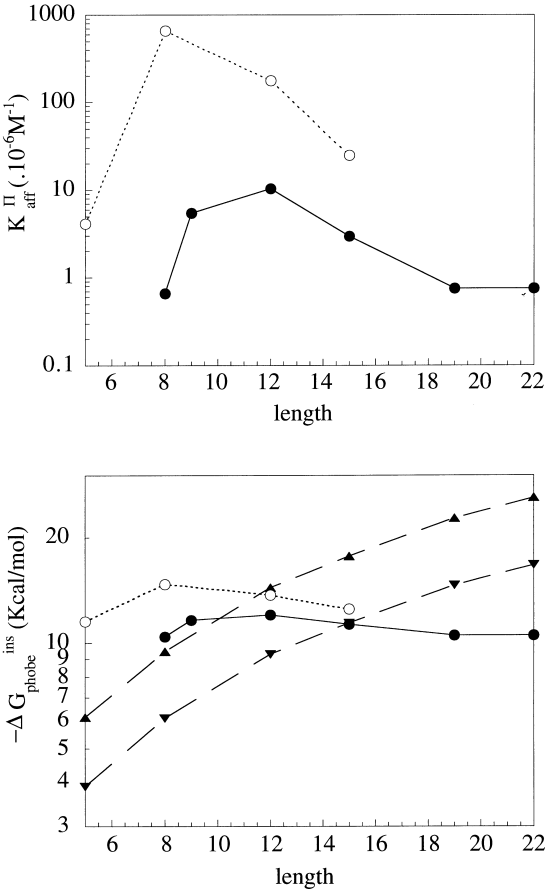

Fig. 9. (Top) Partition constants for the $L_iK_j(i=2j)$ peptides between aqueous phase and DMPC monolayer at different pressures. ●: $\Pi=30$ mN/m; ○: $\Pi=8$ mN/m. (Bottom) Experimental and calculated Gibbs free energy of peptide transfer (ΔG_{ins}^{Π}, ΔG_{ins}^{phobe}) from the aqueous phase to the DMPC monolayer for the $L_iK_j(i=2j)$ peptides. Experimental data (ΔG_{ins}^{Π}): ●: $\Pi=30$ mN/m; ○: $\Pi=8$ mN/m. Calculated data (ΔG_{ins}^{phobe}): ▼: with the Eisenberg hydrophobicity scale (1) [70]; $\Delta G_L=-1.06$ kcal/mole, $\Delta G_{Dns}=-0.81$ kcal/mole; ▲: with the Bull and Breese hydrophobicity scale (2) [77]. $\Delta G_L=-1.65$ kcal/mole, $\Delta G_{Dns}=-1.20$ kcal/mole.

partition at air/water interface and decreases the 'apparent' peptide affinity for the interface.

Neither at 8 nor at 30 mN/m, the K_{aff}^{Π} values, i.e. lipid affinities, evolve monotonously with the peptide hydrophobicity (Fig. 9, top): K_{aff}^{30} increases concurrently with peptide length from 8 to 12 residues (by a factor of 17) then decreases 3.5-fold and 4-fold from 12 to 15 then to 19 and reaches a plateau for the longer peptides (≥19). This evolution can be related to the self-association tendency in solution as documented from fluorescence polarization [38].

At 8 mN/m, K^{8}_{aff} values are higher but vary similarly, the maximum shifts down to shorter peptides. The shorter 5-mer does not insert into the compressed DMPC monolayer while it does at 8 mN/m. $K^{8}_{aff} \approx 60\ K^{30}_{aff}$ for the 8- and 12-mer, and $K^{8}_{aff} \approx 30\ K^{30}_{aff}$ for the 15-mer. This quantitatively documents that peptide incorporation strongly depends on the selected lateral pressure of the lipid.

Gibbs free energies of peptide transfer from the aqueous phase to the phospholipid monolayer, $\Delta G^{\Pi}_{ins} = -RTln(55.5\ K^{\Pi}_{aff})$, are compared to those expected for the free energy of transfer for each peptide from the aqueous solution into an apolar medium. ΔG^{phobe}_{ins} was calculated as $\Delta G^{phobe}_{ins} = \Sigma(\Delta G_{L,Dns})$, assuming that the main driving force for the interaction with a zwitterionic DMPC monolayer is the hydrophobic effect, roughly summing the free energies of transfer of each residue and ignoring the charge effects. Using $\Delta G_{W} \approx \Delta G_{Dns}$ and the values of the consensus Eisenberg hydrophobicity scale [70] leads to ΔG^{phobe}_{ins} (Fig. 9, bottom). Using a more relevant hydrophobicity scale for free energies of transfer from water to the air interface [77] yields significantly larger values. The experimental and calculated ΔG values are in the same range but vary differently (Fig. 9, bottom). Whatever the scale used, the calculated peptide affinity for the interface increases monotonously with length. Experimentally, for short peptides, $-\Delta G^{\Pi}_{ins}$ is higher than calculated ΔG^{phobe}_{ins}, indicating that lipid affinity can be driven by a more complex mechanism than the solely hydrophobic force. For 12- and 15-mers, $-\Delta G^{\Pi}_{ins}$ is quite comparable to what is expected by the theory, and for the longer peptides, $-\Delta G^{\Pi}_{ins}$ always remains weaker. Then, in the case of zwitterionic lipids, the hydrophobic effect is mainly responsible for the affinity and when L≥12, the positive divergence of $-\Delta G^{\Pi}_{ins}$ from the theory is attributable to the documented self-association in buffer solution [38]. The unfavorable contribution of the oligomerization process, ΔG_{ass}, was roughly estimated. It increases with peptide length: 6.4, 12.2 and 15.5 kcal/mol for the 15-, 19- and 22-mers respectively. These values are weaker compared to the −20 kcal/mol obtained for the tetramerization of two amphiphilic 16 residues long peptides designed to mimic 4-helix structure [78] or to the −32 kcal/mol measured for the salt-induced tetramerization in a solution of $(LK_2L_2KL)_2$ [63].

Finally, the comparison of the affinities estimated herein for monolayers to those determined for EPC vesicles by fluorescence [38] shows the same non-monotonous variations versus peptide length, with an optimum for the 15 residues long peptide. Then parameters obtained from monolayers at the air/water interface are relevant for peptide membrane interactions. The difference in the absolute values comes first from the fact that the real equivalent pressure in the SUVs used is probably higher than the 30 mN/m used in the monolayer study.

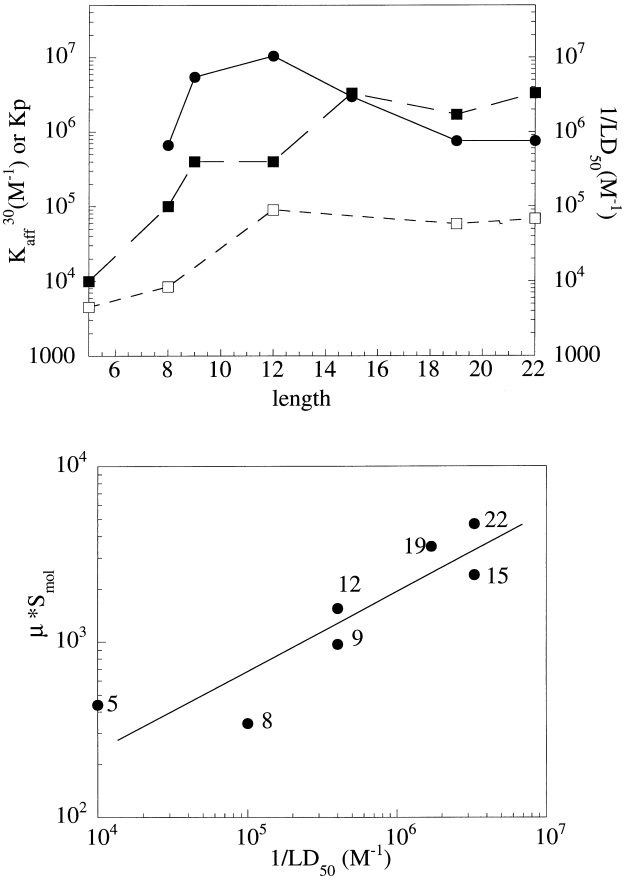

Fig. 10. (Top) Comparison of the variations of the peptide affinities for a DMPC monolayer (K^{30}_{aff}), for EPC bilayers (K_p) and the lytic activity towards erythrocytes ($1/LD_{50}$) versus peptide length for the L_iK_j ($i=2j$) peptides. ●: K^{30}_{aff}; ■: $1/LD_{50}$; □: K_p. (Bottom) Correlation between the physical properties of the peptides determined in the monolayer experiments and the LD_{50} concentration for erythrocytes hemolysis, μ is the calculated hydrophobic moment according to the structure determined at the interface, S_{mol} is the area occupied at the interface from Table 4.

4.6. Parallels with biological lytic activity

The $DnsL_iK_j(i=2j)$ peptides studied here display a high lytic activity towards erythrocytes and liposomes [17,38]. Though the important role of the helicity was often correlated with hemolytic activity, these results support the conclusion that the presence of α-helices is not mandatory for lytic activity, this agrees with the dye leakage from acidic liposomes induced by amphipathic β-sheeted $Ac(SVKV)_n$-$NHCH_3$ ($n=1$–3) or $Ac(KV)_nNHCH_2$ ($n=2$–4) peptides [69].

The monolayer study also leads to a reconsideration of the common and well established lysis mechanism model of α-helix bundles with transmembranous orientation generating channels or holes of variable size in membrane. Neither the β-sheet of the 5-mer, nor the α-helix of the 12-mer is long enough (∼18 Å) to span a bilayer (∼30 Å), even though both are significantly lytic [38]. Furthermore, independent assays using fluorescence show that the energy transfer between W and Dns of ia-$LK_{15}W_{14}$ and $DnsLK_{15}$ could not document the existence of helix bundles in SUV bilayers [38]. Independent calculations also proved that the hydrophobic part of the amphiphilic α-helix can penetrate the outer leaflet down to the C_5 position without giving rise to any helix bundle [75] and that a helix running parallel to the bilayer plane can be comfortably accommodated within the interface [75]. Then lysis induced by $DnsL_iK_j(i=2j)$ could primarily be due to peptides lying flat on the outer leaflet of membrane without any secondary structure requirement. This fits with 'carpet' [21] or 'raft' [20] models documented for natural lytic peptides like melittin [17] or magainins [23,24]. The immediate significant and asymmetric surface increase leads to huge mechanical constraints and the local defects in lipid organization will then result in transient failure of the membrane permeability barrier.

The affinities determined either on DMPC monolayer (K_{aff}^{30}) or on EPC SUV bilayer (K_p) and the lethal dose for 50% hemolysis [38] evolve rather similarly versus peptide length (Fig. 10, top); the lipid affinities and the lytic activity increase with peptide lengths up to 12–15 residues then reach a plateau or slightly decrease. However, even if lipid affinity is a key parameter which first governs the interaction with biological membrane, there is no quantitative correlation with lytic activity (not shown). Then other parameters have to be considered to explain the evolution of biological activity versus peptide length. Lytic activity correlates quite well with the product $\mu \times S_{mol}$ (Fig. 10, bottom) where μ is the hydrophobic moment calculated with the peptide structure determined by PMIRRAS. Then μ, which takes into account the influence of the hydrophobicity, the topology and the real structure when bound, conformation and the orientation at the interfaces, of the $L_iK_j(i=2j)$ peptides is more adequate to yield for the evolution of the lytic activity than the lipid affinity alone. This also shows that the lytic activity can be reasonably well anticipated over a three log scale by intrinsic parameters of peptides. The lipid affinity and the number of bound molecules which are of course essential to obtain a significant activity are not the sole limiting modulators of lytic activity.

Acknowledgements

We are pleased to acknowledge Dr. Klaus Büttner at Fournier Pharma GmbH, Heidelberg, for providing some of the peptides used herein and Wilfrid Neri for skilful purification of short peptides. This work was supported in part by CNRS program GDR790.

References

[1] R.M. Kini, H.J. Evans, Int. J. Peptide Protein Res. 34 (1989) 277–286.
[2] W.F. De Grado, G.F. Musso, M. Lieber, E.T. Kaiser, F.J. Kézdy, Biophys. J. 37 (1982) 329–338.
[3] M.T. Tosteson, S.J. Holmes, M. Razin, D.C. Tosteson, J. Membr. Biol. 87 (1985) 35–44.
[4] C.E. Dempsey, Biochim. Biophys. Acta 1031 (1990) 143–161.
[5] G. Colaccico, M.K. Basu, A.R. Buchelew, A.W.J. Berheimer, Biochim. Biophys. Acta 465 (1977) 378–390.
[6] M. Bhakoo, T.H. Birkbeck, J.H. Freer, Biochemistry 21 (1982) 6883–6889.
[7] G. Signor, S. Mammi, E. Peggion, H. Ringsdorf, A. Wagenknecht, Biochemistry 33 (1994) 6659–6670.
[8] R. Maget-Dana, M. Ptak, Biophys. J. 73 (1997) 2527–2533.
[9] L.K. Tamm, in: S. White (Ed.), Membrane Protein Structure, Oxford University Press, Oxford, 1994, pp. 283–313.

[10] E. Schröder, K. Lübke, M. Lehmann, I. Beetz, Experientia 27 (1971) 764–765.
[11] P. Bougis, H. Rochat, G. Piéroni, R. Verger, Biochemistry 20 (1981) 4915–4920.
[12] P. Ash, R.C. Hider, A.A. Menez, A.G. Wunderer, Biochim. Biophys. Acta 669 (1981) 231–235.
[13] M. Grandbois, J. Dufourcq, C. Salesse, Thin Solid Films 284 (1996) 743–747.
[14] G. Saberwal, R. Nagaraj, Biochim. Biophys. Acta 1197 (1994) 109–131.
[15] T. Kiyota, S. Lee, G.V. Sugihara, Biochemistry 35 (1996) 13196–13204.
[16] I. Cornut, K. Büttner, J.L. Dasseux, J. Dufourcq, FEBS Lett. 349 (1994) 29–33.
[17] I. Cornut, B. Desbat, J.M. Turlet, J. Dufourcq, Biophys. J. 70 (1996) 305–312.
[18] M. Dathe, T. Wieprecht, H. Nikolenko, L. Handel, M.L. Maloy, D.L. Mc Donald, M. Beyerman, M. Bienert, FEBS Lett. 403 (1997) 208–212.
[19] S. Castano, B. Desbat, I. Cornut, P. Méléard, J. Dufourcq, Lett. Peptide Sci. 4 (1997) 195–200.
[20] G. Raghunathan, P. Seetharamulu, B.R. Brooks, H.R. Guy, Proteins 8 (1990) 213–225.
[21] Y. Shai, Trends Biochem. Sci. 20 (1995) 460–464.
[22] B. Bechinger, J. Membr. Biol. 156 (1997) 197–211.
[23] B. Bechinger, M. Zasloff, S.J. Opella, Protein Sci. 2 (1993) 2077–2084.
[24] K. Matsuzaki, O. Murase, H. Tokuda, S. Funakoshi, N. Fujii, K. Miyajima, Biochemistry 33 (1994) 3342–3349.
[25] H. Vogel, F. Jähnig, V. Hofmann, J. Stümpel, Biochim. Biophys. Acta 733 (1983) 201–209.
[26] J.W. Brauner, R. Mendelsohn, F.G. Prendergast, Biochemistry 26 (1987) 8151–8158.
[27] Y.P. Zhang, R.N.A.H. Lewis, R.S. Hodges, R.N. McElhaney, Biophys. J. 68 (1995) 847–857.
[28] R. Brasseur, J. Biol. Chem. 266 (1991) 16120–16127.
[29] S. Frey, L.K. Tamm, Biophys. J. 60 (1991) 922–930.
[30] R. Mendelsohn, J.W. Brauner, A. Gericke, Annu. Rev. Phys. Chem. 46 (1995) 305–334.
[31] R.A. Dluhy, J. Phys. Chem. 90 (1986) 1373–1379.
[32] C.R. Flack, J.W. Brauner, J.W. Taylor, R.C. Baldwin, R. Mendelsohn, Biophys. J. 67 (1994) 402–410.
[33] A. Gericke, C.R. Flach, R. Mendelsohn, Biophys. J. 73 (1997) 492–499.
[34] D. Blaudez, J.M. Turlet, J. Dufourcq, D. Bard, T. Buffeteau, B. Desbat, J. Chem. Soc. Faraday Trans. 92 (1996) 525–530.
[35] B. Pastrana-Rios, S. Taneva, K.M.W. Keough, A.J. Mautone, R. Mendelsohn, Biophys. J. 69 (1995) 2531–2540.
[36] M. Boncheva, H. Vogel, Biophys. J. 73 (1997) 1056–1072.
[37] C.R. Flach, F.G. Prendergast, R. Mendelsohn, Biophys. J. 70 (1996) 539–546.
[38] S. Castano, I. Cornut, K. Büttner, J.L. Dasseux, J. Dufourcq, Biochim. Biophys. Acta 1416 (1999) 161–175.
[39] E. Perez-Paya, J. Dufourcq, L. Braco, C. Abad, Biochim. Biophys. Acta 1323 (1997) 223–236.
[40] A.F. Mingotaud, C. Mingotaud, L.K. Patterson, Handbook of Monolayers, Vol. 2, Harcourt Brace Jovanovitch, San Diego, CA, 1992.
[41] D. Blaudez, T. Buffeteau, J.C. Cornut, B. Desbat, N. Escafre, M. Pezolet, J.M. Turlet, Thin Solid Films 242 (1994) 146–150.
[42] G. Sessa, J.H. Freer, G. Colacicco, G. Weismann, J. Biol. Chem. 244 (1969) 3575–3582.
[43] V.S. Gevod, K.S. Birdi, Biophys. J. 45 (1984) 1079–1083.
[44] T. Miyazawa, Infrared Spectra and Helical Conformations, Marcel Dekker, New York, 1967.
[45] B. Pastrana, A.J. Mautone, R. Mendelsohn, Biochemistry 30 (1991) 10058–10064.
[46] E. Goormaghtigh, V. Cabiaux, J.M. Ruysschaert, in: H.J. Hilderson, G.B. Ralston (Eds.), Subcellular Biochemistry: Physicochemical Methods in the Study of Biomembranes, Vol. 23, Plenum Press, New York, 1994, pp. 405–450.
[47] F. Dousseau, M. Pezolet, Biochemistry 29 (1990) 8771–8779.
[48] J.L.R. Arrondo, A. Muga, M.J. Castresana, F.M. Goni, Prog. Biophys. Mol. Biol. 59 (1993) 23–56.
[49] P.H. Axelsen, B.K. Kaufman, R.N. MacElhaney, R.N.A.H. Lewis, Biophys. J. 69 (1995) 2770–2781.
[50] E. Goormaghtigh, V. Cabiaux, J.M. Ruysschaert, Eur. J. Biochem. 193 (1990) 409–420.
[51] W.K. Surewicz, T.M. Stepanick, A.G. Szabo, H.H. Mantsch, J. Biol. Chem. 263 (1988) 786–790.
[52] W.K. Surewicz, H.H. Mantsch, D. Chapman, Biochemistry 32 (1993) 389–394.
[53] S. Krimm, J. Bandekar, Adv. Protein Chem. 38 (1986) 181–364.
[54] P.I. Haris, D. Chapman, Trends Biochem. Sci. 17 (1992) 328–333.
[55] S.A. Tatulian, L.R. Jones, L.G. Reddy, D.L. Stokes, L.K. Tamm, Biochemistry 34 (1995) 4448–4456.
[56] S. Krimm, W.C. Reisdorf, Faraday Discuss. 99 (1994) 181–197.
[57] F.N. Fu, D.B. De Oliveira, W.R. Trumble, H.K. Sarkar, B.R. Singh, Appl. Spectrosc. 48 (1994) 1432–1441.
[58] T. Buffeteau, B. Desbat, Appl. Spectrosc. 43 (1989) 1027–1032.
[59] D. Marsh, Biophys. J. 72 (1997) 2710–2718.
[60] R.A. Demel, W.S.M.G. van Kessel, R.F.A. Zwaal, B. Roelfsen, L.L.M. van Deenen, Biochim. Biophys. Acta 406 (1975) 97.
[61] S.H. Portlock, Y. Lee, J. Tomich, L.K. Tamm, J. Biol. Chem. 267 (1992) 11017–11022.
[62] E. Goormaghtigh, V. Cabiaux, J.M. Ruysschaert, in: H.J. Hilderson, G.B. Ralston (Eds.), Subcellular Biochemistry: Physicochemical Methods in the Study of Biomembranes, Vol. 23, Plenum Press, New York, 1994, pp. 363–403.
[63] W.F. De Grado, J.D. Lear, J. Am. Chem. Soc. 107 (1985) 7684–7689.
[64] J.H. Freer, T.H. Birkbeck, M. Bhakoo, in: J.E. Alouf (Ed.), Bacterial Protein Toxins, Academic Press, London, 1984, pp. 181–189.

[65] D.J. Ciesla, D.E. Gilbert, J. Feigon, J. Am. Chem. Soc. 113 (1991) 3957–3961.
[66] J. Dufourcq, W. Neri, N. Henry-Toulme, FEBS Lett. 421 (1998) 7–11.
[67] M. Narita, Y. Tomotake, S. Isohawa, T. Matsuzawa, T. Miyauchi, Macromolecules 17 (1984) 1903–1906.
[68] K.H. Altmann, A. Florsheimer, M. Mutter, Int. J. Peptide Protein Res. 27 (1986) 314–319.
[69] S. Ono, S. Lee, H. Mihara, Y. Aoyagi, T. Kato, N. Yamasaki, Biochim. Biophys. Acta 1022 (1990) 237–244.
[70] D. Eisenberg, R.M. Weiss, T.C. Terwilliger, Nature 299 (1982) 371–374.
[71] K.E. Krebs, M.C. Phillips, FEBS Lett. 175 (1984) 263–266.
[72] S.J. Opella, J. Gesell, B. Bechinger in: R.M. Epand (Ed.), The Amphipathic Helix, CRC Press, Boca Raton, FL, 1993, pp. 87–106.
[73] R.E. Dickerson, I. Geis, The Structure and Action of Proteins, Harper and Row, New York, 1969.
[74] J.A. Reynaud, J.P. Grivet, D. Sy, Y. Trudelle, Biochemistry 32 (1993) 4997–5008.
[75] S.H. White, W.C. Winley, Curr. Opin. Struct. Biol. 4 (1994) 79–86.
[76] T.E. Creighton, Proteins, Structure and Molecular Properties, W.H. Freeman and Company, New York, 1996.
[77] B.H. Bull, K. Breese, Arch. Biochem. Biophys. 161 (1974) 665–670.
[78] S.P. Ho, W.F. De Grado, J. Am. Chem. Soc. 109 (1987) 6751–6758.